

1995120866

48599?
15p.**BALL BEARING VIBRATIONS
AMPLITUDE MODELING AND TEST COMPARISONS**

Richard A. Hightower III* and Dave Bailey*

ABSTRACT

Bearings generate disturbances that, when combined with structural gains of a momentum wheel, contribute to induced vibration in the wheel. The frequencies generated by a ball bearing are defined by the bearing's geometry and defects. The amplitudes at these frequencies are dependent upon the actual geometry variations from perfection; therefore, a geometrically perfect bearing will produce no amplitudes at the kinematic frequencies that the design generates. Because perfect geometry can only be approached, emitted vibrations do occur. The most significant vibration is at the spin frequency and can be balanced out in the build process. Other frequencies' amplitudes, however, cannot be balanced out.

Momentum wheels are usually the single largest source of vibrations in a spacecraft and can contribute to pointing inaccuracies if emitted vibrations ring the structure or are in the high-gain bandwidth of a sensitive pointing control loop. It is therefore important to be able to provide an a priori knowledge of possible amplitudes that are singular in source or are a result of interacting defects that do not reveal themselves in normal frequency prediction equations.

This paper will describe the computer model that provides for the incorporation of bearing geometry errors and then develops an estimation of actual amplitudes and frequencies. Test results were correlated with the model.

A momentum wheel was producing an unacceptable 74 Hz amplitude. The model was used to simulate geometry errors and proved successful in identifying a cause that was verified when the parts were inspected.

INTRODUCTION

Vibration in spacecraft has always been of concern when considering component life and performance issues. Of particular concern is the effect on pointing accuracies of instruments that must perform despite emitted vibrations from other on-board devices.

* Honeywell Inc., Satellite Systems Operation, Glendale, Arizona

Momentum wheels provide momentum control for space vehicles. The wheel is supported by conventional ball bearings, which generate their own vibration due to normal manufacturing geometry errors and/or defects. To gain a better understanding of how these geometry errors and defects contribute to induced vibration from the bearings, a model was developed and applied to study these motions. This model is actually an extension of a static model developed to analyze mounted and operating preload, ball loading, and contact stresses.

MODEL DESCRIPTION

The **Motion Model** was developed as an analytical tool that could be utilized to predict bearing motion. If bearing motion could be predicted, then ultimately individual bearing parts could be matched to yield bearing assemblies (bearing pairs in the momentum wheel application) that produce minimal bearing motions.

The Motion Model is a quasistatic model that actually analyzes bearing motion in 512 (or less if desired) incremental steps as a static model. This number of steps was determined as sufficient to yield adequate frequency resolution over the frequency spectrum of interest (0 - 200 Hz). The data from these 512 steps is run through a discrete Fast Fourier Transform (FFT) Routine, developed by Dave Bailey, Honeywell Satellite Systems Operation (SSO), to yield a frequency spectrum of radial and axial amplitudes. The FFT Routine requires 2^n steps to generate a spectrum from the model data. The number of steps selected is divided by the number of inner ring (e.g., shaft) rotations. The number of shaft rotations input into the model represents the number of inner ring rotations that will bring the inner ring and balls back to their original starting position, taking into account nominal bearing geometry. For the 305 size bearing referenced in this paper, 19 inner ring (e.g., shaft) rotations are required.

Motions generated by the model include radial (designated k & v by the model) and axial (designated h) forces and deflections. Figure 1 shows the sign convention used.

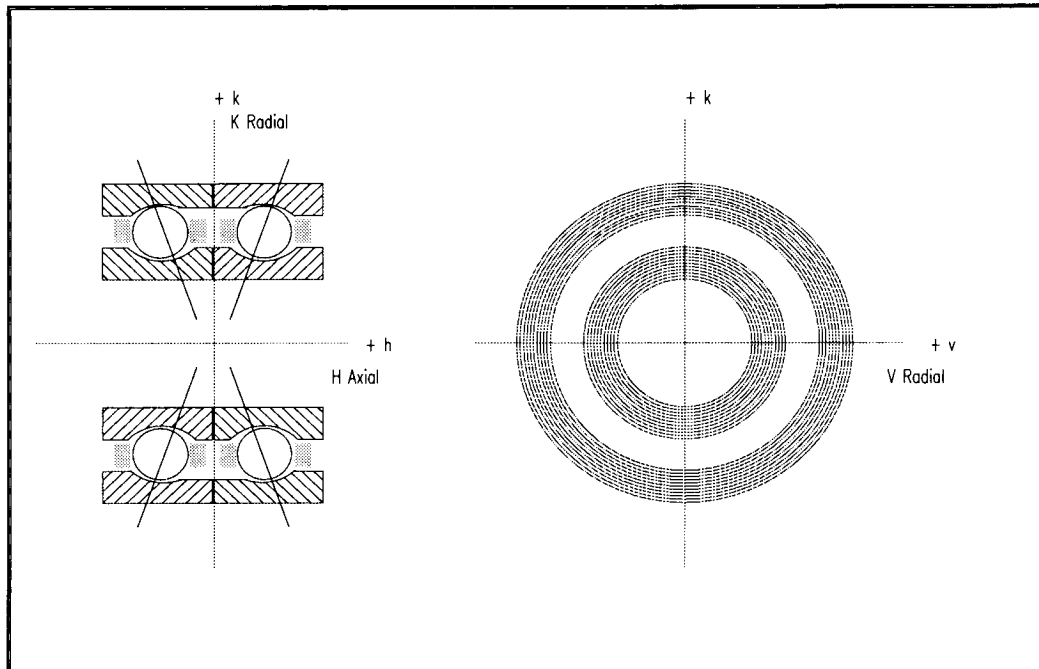


Figure 1. Motion Model Sign Convention

Model Input Description. Bearing nominal geometry, measured bearing geometry errors, and mounting interfaces are accepted as inputs into the model to predict shaft motions under 0 or 1g loading conditions. Bearing geometry is initially entered into the input file and is used by the model to determine preload. The following bearing geometry parameters are inputs to the model. Actual values for the 305 size bearing discussed in this paper are listed.

305 Size

Bearing outside diameter	62.0 mm (2.4409 in.)
Bearing bore	25.0 mm (0.9843 in.)
Preload (unmounted)	5.44 kg (12 lbm)
Free contact angle	13.66 deg
Bearing width	17.0 mm (0.6693 in.)
Race curvature	Proprietary
# balls	10
Ball diameter (nominal)	11.9 mm (0.46875 in.)
Ball pitch diameter	44.3 mm (1.743 in.)

Bearing geometry errors that can be input into the model follow:

- ✓ Race Node Eccentricities (defined as the number of points out-of-round)

Input Options - 1, 2, 3, or 4 Node

- Node 1 is a simple eccentricity, i.e., the bore axis offset from the race axis
- Node 2 is a 2 point out-of-round, i.e., oval shaped
- Node 3 is a 3 point out-of-round
- Node 4 is a 4 point out-of-round

Eccentricity values can be input for:

- Inner and/or outer radial eccentricity
- Inner and/or outer axial eccentricity

- ✓ Race Talyrond Data (radial only)
 - Digitized data. A sample plot of a typical error data file is shown in Figure 2.

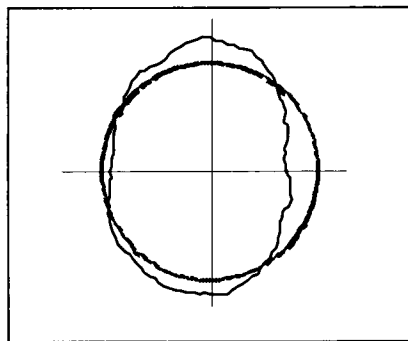
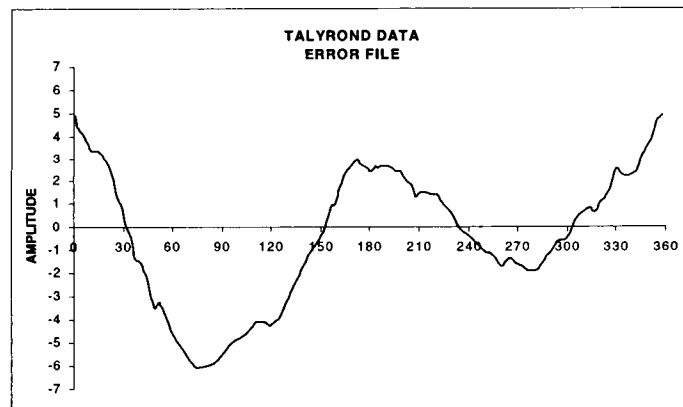


Figure 2. Talyrond Error Plot

- ✓ Contact Angle difference (row 1 versus row 2)
- ✓ Ball Geometry Errors
 - Size Errors generally input as a random ball size deviation
Specific ball size deviations can also be entered
 - Spacing Errors input for biased cage applications

Program-generated geometry errors from previous error inputs, together with the measured Talyrond errors, are summed and input into the main model for the motion analysis.

In addition to the above inputs, the model will also allow the inner and/or outer rings to be "clocked" relative to each other. This clocking allows the model to analyze motions for various face-to-face alignments of the bearing rings. In addition, the effect of phasing the inner or outer ring radial eccentricities relative to the axial eccentricities at specified angles can be investigated.

Figure 3 is a sample input file¹ used by the Motion Model.

Motion plots are generated by the model and are shown as the number of steps versus deflection amplitude. Information that can be extracted from these plots includes not only deflection ranges but motion phase information amongst the three components. Figure 4 is an example of a motion plot.

In addition to motion plots, frequency spectrum plots versus radial and axial amplitudes can also be generated. Figure 5 is an example of a frequency plot.

Other plots that can be generated include force (N) and acceleration (g's) versus frequency.

MODEL VALIDATION

Validation of the Motion Model was an important first step towards gaining an understanding of how the model worked and determining what key bearing parameters needed to be included in the model. A program verification test matrix was therefore developed to review motion and FFT plots generated by the model and to ensure that the test cases agreed with expected results.

Analytical Test Matrix. The intent of the test matrix was to look at each bearing geometry error independently and combined, to review the motion and FFT output of each test case, and to determine if the output was as expected.

The analytical test matrix included:

- Perfect part geometries
- Radial and axial eccentricities for 1 node to 4 node geometry errors
- Ball size errors
- Ball spacing errors
- Two balls missing
- Shaft unbalance forces
- 0g (space environment) and 1g (ground environment) loading

¹ Inputs shown not specific to this paper.

```

?PROBLEM SET DESCRIPTION .....|
61071gF3 - VER 5.2 JULY 5,1991 RUN DATE 08/09/91
?DESCRIPTION .....|
1G GRAVITY CASE - BIASED CAGE - OUTER CLOCKED 90 INNER EVERY 30 deg
?NO ROWS |?DF/DT/DB|?THRUST |?RADIAL |?APHA/MOM|? RPM |? STEPS |?CONTROL |
-2. -1. 0.0 20. 2000. 512. 1.
?STRADDLE|?PRELOAD |?CASE |?FMU-PRLD|?RATE |?GAP |?FLUSH |?FILM |
.6693 12.0 1. .15 -.000005
?FMUS |?FMUL |?FMUC |?L-VIS CS|?L-QUAN |?CLEAR |?XRUN |?NUSE |
.07 .07 .07 140. .13 .010
?SH TURNS|?SHAFT WT|?UNBAL |?UNBA ANG|?ITER_TOL|?DIFF_CA |?VRADIAL |?TEST |
19. 0. 0. .025 -.140
? ROW NO |?#-BALLS |?BALL DIA|?FREE CA |? E |? FI |? FO |? BGAP |
1. 10.0 .46875 13.66 1.743 .54 .55
?IR PRESS |?IR HD/D |?IR-DAM/D|?IR-WIDTH|?SHAFT ID|?BRG BORE|?IR-CLAMP|?IRC-FMU |
.000200 .26 .26 .6693 2.4409 5. .9843 100. .1
?OR PRESS |?OR HD/D |?OR-DAM/D|?OR-WIDTH|? BRG OD |? HSG OD |?OR-CLAMP|?ORC-FMU |
-.00037 .26 .26 .6693 2.4409 5. 100. .1
?E-SHAFT |?E-BRG |?E-HSG |?PR-SHAFT|?PR-BRG |?PR-HSG |DENSITY |? DELR |
32.E6 32.E6 32.E6 .32 .32 .30 .150
?TC-SHAFT|?TC-BRG |?TC-HSG |?OT-SHAFT|?OT-IR |?OT-OR |?OT-HSG |? DELH |
7.0E-6 7.5E-6 6.2E-6 80. 80. 70. 75.
-----ROW 1 GEOMETRY ERRORS (MICROINCHES) ---|RADIAL TO AXIAL DEG|IR RADIAL|
?NODE |?IR RAD |?OR RAD |?IR AXIAL|?OR AXIAL|?PHASE IR|PHASE OR |?SHIFT |
1. 30.0 40.0 -30.0 30.0
2.
3.
4.
?SHIFT IR|?SHIFT OR| | |?IR FILE |?OR FILE |
90. IR721FX.RND OR520FX.RND
? NSIR |? NSOR |?BSIZE |? |? |? |
12.0 1.0 0.000005
----- BALL SPACING ERRORS (degrees) -----
?BALL1 |?BALL2 |?BALL3 |?BALL4 |?BALL5 |?BALL6 |?BALL7 |?BALL8 |?BALL9 |?BALL10|
?BALL11|?BALL12|?BALL13|?BALL14|?BALL15|?BALL16|?BALL17|?BALL18|?BALL19|?BALL20|
----- BALL DIAMETER ERRORS (micro-inches) -----
?BALL1 |?BALL2 |?BALL3 |?BALL4 |?BALL5 |?BALL6 |?BALL7 |?BALL8 |?BALL9 |?BALL10|
?BALL11|?BALL12|?BALL13|?BALL14|?BALL15|?BALL16|?BALL17|?BALL18|?BALL19|?BALL20|
-----ROW 2 GEOMETRY ERRORS (MICROINCHES) ---|RADIAL TO AXIAL DEG|IR RADIAL|
?NODE |?IR RAD |?OR RAD |?IR AXIAL|?OR AXIAL|?PHASE IR|PHASE OR |?SHIFT |
1. 20.0 45.0 30.0 -30.0
2.
3.
4.
?SHIFT IR|?SHIFT OR| | |?IR FILE |?OR FILE |
IR672FX.RND OR353FX.RND
? NSIR |? NSOR |?BSIZE |? |? |? |
1.0 1.0 0.000005
----- BALL SPACING ERRORS (degrees) -----
?BALL1 |?BALL2 |?BALL3 |?BALL4 |?BALL5 |?BALL6 |?BALL7 |?BALL8 |?BALL9 |?BALL10|
?BALL11|?BALL12|?BALL13|?BALL14|?BALL15|?BALL16|?BALL17|?BALL18|?BALL19|?BALL20|
----- BALL DIAMETER ERRORS (micro-inches) -----
?BALL1 |?BALL2 |?BALL3 |?BALL4 |?BALL5 |?BALL6 |?BALL7 |?BALL8 |?BALL9 |?BALL10|
?BALL11|?BALL12|?BALL13|?BALL14|?BALL15|?BALL16|?BALL17|?BALL18|?BALL19|?BALL20|

```

Figure 3. Model Input File

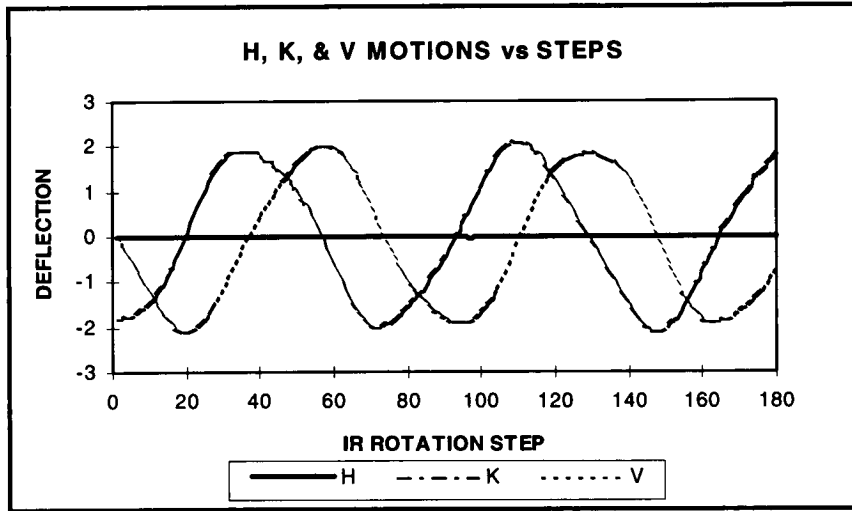


Figure 4. Motion Plot

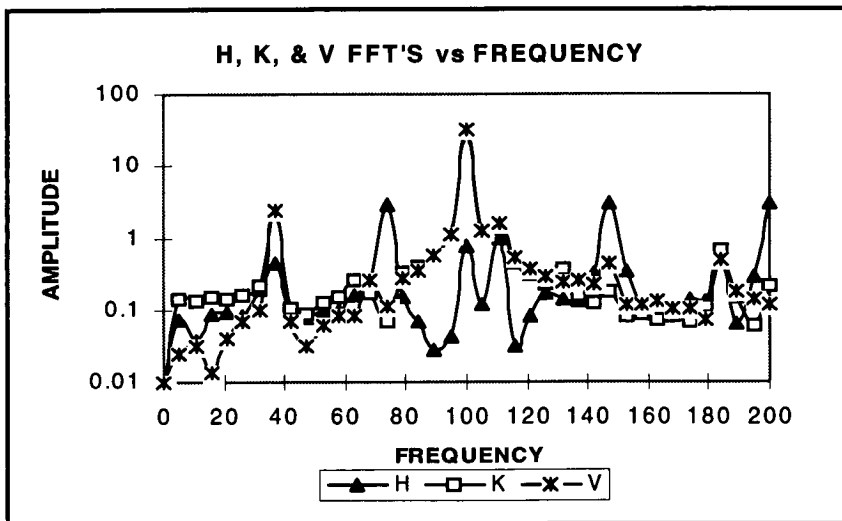


Figure 5. Frequency Plot

A total of 122 test cases were run and reviewed.

Several iterations of these test cases were completed because each iteration revealed additional model errors and identified model enhancements. Finally, all 122 test case results were considered acceptable and it was concluded that the model was valid.

Figures 6 and 7 are shown to illustrate the sensitivity of the model to inputted geometry errors. Figure 6 shows a frequency plot for a 0.10 μm (4 $\mu\text{in.}$) cosine ball size distribution error input; no other geometry errors were input. As expected, the model generated a disturbance at the ball group frequency, a 37 Hz peak of 0.10 μm (4 $\mu\text{in.}$) amplitude.

Figure 7 is an output plot for the same cosine ball size distribution and a 0.09 kg (0.2 lbm) shaft unbalance force applied. Note the motion response at the 100 Hz spin frequency.

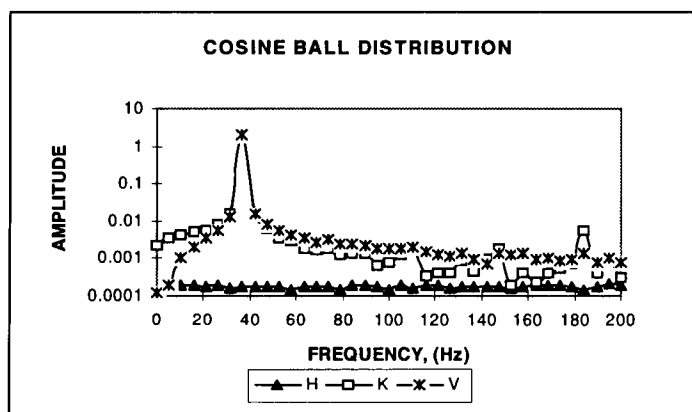


Figure 6. Cosine Ball Distribution

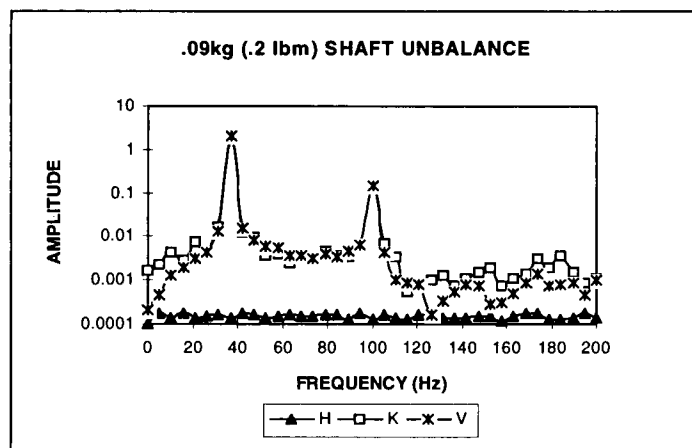


Figure 7. Shaft Unbalance

BEARING DISTURBANCES

Two frequencies have been identified as being of particular interest in the investigation of bearing disturbance effects on momentum wheels. These frequencies are 74 and 100 Hz. A momentum wheel was producing an unacceptable 74 Hz axial disturbance. The model was used to simulate geometry errors and identify a cause.

Frequency Drivers. The model was run using actual measured data from a 305 size bearing pair to investigate effects on bearing motion due to inner and outer ring clocking and phasing. This data included measured contact angle, face stickout, and bore diameter. In addition, axial runout and unmounted preload was input to the model for the bearing pair. Inspection data for each bearing ring (inner and outer) included race/bore radial runout and race radial roundness. Talyrond plots of the individual rings were digitized and converted to error files for the model. A $\pm 0.13 \mu\text{m}$ ($\pm 5 \mu\text{in.}$) random ball size error distribution was input into the model, which is the size variation specified for Anti-Friction Bearing Manufacturers Association (AFBMA) Grade 3 balls. Also, ball position errors were included to account for biased cage geometry effects.

Cases were run for 0g and 1g loading.

Table 1 lists the cases that were run in the model, the parameters that were varied, and the effect on the Model output.

Table 1. Actual Bearing Results

Case	Parameter Varied	Model Results
1 (0g) 2 (1g)	Inner rings clocked every 30°	Negligible change in amplitudes at all frequencies
3 (0g)	Same as above + Same size balls	Negligible change in amplitudes
4 (0g) 5 (1g)	Inner rings clocked every 30° for every 30° clocking of outer ring	Negligible change in amplitudes
6 (0g) 7 (1g)	Phase radial to axial inner ring ecc. 90° for every 90° phasing of radial to axial outer ring ecc. (row 1 only)	Negligible change in amplitudes
8 (0g) 9 (1g)	Shift row 1 rings $+2.54 \mu\text{m}$ ($+100 \mu\text{in.}$), row 2 rings $-2.54 \mu\text{m}$ ($-100 \mu\text{in.}$)	Large increase in axial amplitudes at 74 and 100 Hz

Results from these runs follow:

- ◆ Inner ring clocking has no effect on amplitudes
- ◆ Outer ring clocking has no effect on amplitudes
- ◆ Random ball size change has a small effect on amplitudes at 37 Hz
- ◆ Phasing of eccentricities has a minimal effect on amplitudes at 100 Hz
- ◆ Loading (0g versus 1g) has an effect on 100 Hz axial and 74 Hz radial components

In completing the model verification test runs, bearing disturbance frequencies, geometry error input, and the component drive (radial or axial), relationships were noted. Table 2 summarizes the relationship of these factors.

Table 2. Bearing Disturbances

Frequency	Disturbance Causes	Component
74 Hz	Ball size (random)	Radial/Axial
	Ball position (biased cage)	Radial
	Outer ring geometry combined with ball size variation	Radial
	Outer ring geometry combined with ball size and ball position	Radial/Axial
100 Hz	1 large/9 small balls	Radial
	Inner race axial eccentricity (node 1)	Radial/Axial
	Inner race radial eccentricity (node 1)	Radial/Axial
	Rotor unbalance force	Radial

From Table 2 it is evident that 74 Hz axial motion is controlled by ball group symmetry and/or outer race geometry.

Momentum Wheel Amplitude Prediction. The most likely cause of the 74 Hz axial bearing motion generated in the momentum wheel is outer ring geometry errors. One scenario that could cause this geometry error is the bearing cartridge "squeezing" the bearing outer ring. This squeezing is actually a two-point interference fit between the bearing cartridge and the bearing outer ring. It was theorized that the cartridge had possibly become egg-shaped (i.e., node 2 error) as a result of slots that were cut into the cartridge to accommodate other hardware. These slots could have stress-relieved the part, allowing the cartridge to deform and squeeze the outer rings of the bearings.

The outer ring squeeze was modeled as a 2 node radial geometry error in row 1 and row 2 of the bearing outer rings. Figure 8 shows the node 2 error relative to a "perfect" ring.

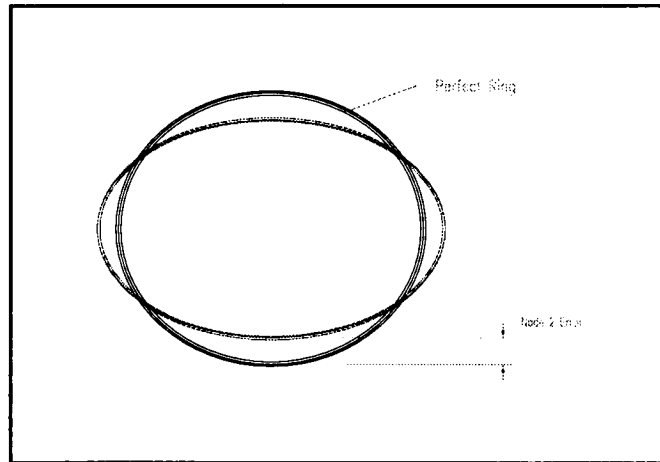


Figure 8. Outer Ring Node 2 Error

Bearing inspection data for the bearings mounted in the momentum wheel was used for geometry error inputs. These inputs, in addition to mounting and loading parameters, are as follows:

- ◆ Ball position error biased cage
 - ◆ Random ball size $\pm 0.13 \mu\text{m}$ ($\pm 5 \mu\text{in.}$)
 - ◆ Node 1 eccentricity
- | | |
|-------|---|
| Row 1 | 0.76 μm (30 $\mu\text{in.}$) inner radial |
| | 1.02 μm (40 $\mu\text{in.}$) outer radial |
| | 0.76 μm (30 $\mu\text{in.}$) inner axial |
| | 0.76 μm (30 $\mu\text{in.}$) outer axial |
| Row 2 | 0.51 μm (20 $\mu\text{in.}$) inner radial |
| | 1.14 μm (45 $\mu\text{in.}$) outer radial |
| | 0.76 μm (30 $\mu\text{in.}$) inner axial |
| | 0.76 μm (30 $\mu\text{in.}$) outer axial |
- ◆ Talyrd data digitized data
 - ◆ Bore/Shaft interference 2.54 μm (100 $\mu\text{in.}$)
 - ◆ Bearing OD clearance 9.40 μm (370 $\mu\text{in.}$)
 - ◆ 1g loading

Several cases were modeled to compare the axial amplitudes for different node 2 error values. Cases were run with equal node 2 errors in both rows, 2x error in row 1 versus row 2, 3.81 μm (150 $\mu\text{in.}$) error difference in row 1 versus row 2, and 7.62 μm (300 $\mu\text{in.}$) error in row 1 versus row 2. These inputs are summarized in Table 3.

Table 3. Node 2 Error Inputs

Case	Node 2 Error μm ($\mu\text{in.}$)	
	Row 1	Row 2
Baseline	0	0
Row 1 & 2	7.62 (300)	7.62 (300)
Row 1 & 2	5.08 (200)	5.08 (200)
Row 1 & 2	2.54 (100)	2.54 (100)
Row 1 & 2	0.76 (30)	0.76 (30)
Row 1 & 2	0.38 (15)	0.38 (15)
Split Row 1 & 2	7.62 (300)	3.81 (150)
Split Row 1 & 2	5.08 (200)	2.54 (100)
Split Row 1 & 2	2.54 (100)	1.27 (50)
Split Row 1 & 2	0.76 (30)	0.38 (15)
Split Row 1 & 2	0.38 (15)	0.19 (7)
Split 150 μin	3.81 (150)	0 (0)
Split 150 μin	7.62 (300)	3.81 (150)
Split 150 μin	11.43 (450)	7.62 (300)
Row 1 only	7.62 (300)	0

Figure 9 shows the results of the 2 node geometry effects for each of the cases. Figure 10 is a plot of axial amplitude versus frequency.

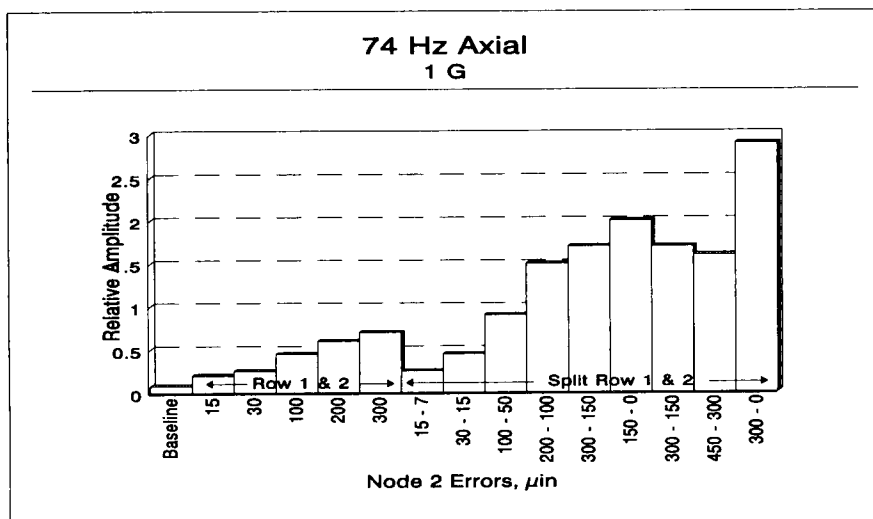


Figure 9. 2 Node Results

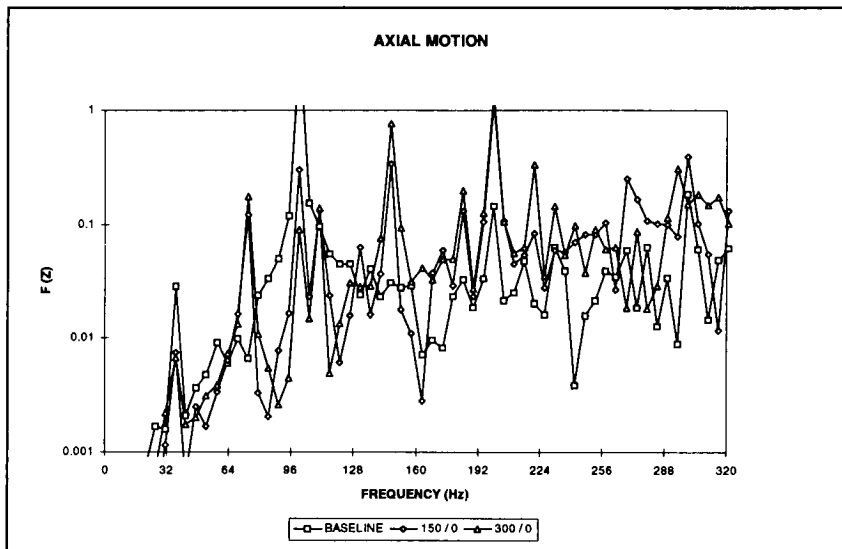


Figure 10. Frequency Plot

Axial motion is largest for the $7.62 \mu\text{m}$ ($300 \mu\text{in.}$) node 2 error difference in row 1 versus row 2. The cases where there is a $3.81 \mu\text{m}$ ($150 \mu\text{in.}$) difference in node 2 errors between row 1 and row 2 show a **decrease** in amplitude as the absolute values of the errors are increased equally for each row. This is expected because the spring rates of each bearing are increasing as the radial squeezing increases in both rows. As the difference in node 2 errors between rows increases, the axial amplitude increases. The cases where the node errors are equal in both rows have relatively low axial amplitudes, even for a $7.62 \mu\text{m}$ ($300 \mu\text{in.}$) error.

An interesting general result in pursuing the 74 Hz disturbance is that axial motions at 100 Hz are driven by external radial loads.

From this data, it was concluded that significant axial motion at 74 Hz can be generated by outer ring node 2 errors together with ball position and size errors, particularly when the error difference between rings is large [$>2.54 \mu\text{m}$ ($100 \mu\text{in.}$)]; therefore, the next step was to inspect both cartridges from the momentum wheel.

TEST RESULTS

Parts Inspection. As a result of the model predictions for the possible source of the 74 Hz axial disturbance, the bearing cartridges were inspected on the momentum wheel producing the axial disturbance. One of the two bearing cartridges was found to be out-of-round. Measurements of the bearing outer ring and cartridge bore confirmed that there was an interference.

Wheel Test Results. A series of tests were conducted to verify that the out-of-round cartridge was indeed the driver. Frequency data was taken with the 305 bearing pair installed in the out-of-round cartridge and again with the bearings installed in a round cartridge. The test was repeated with the bearings installed in the out-of-round cartridge to check repeatability of the measurements. Frequency output data for the out-of-round cartridge is shown in Figure 11, while Figure 12 illustrates frequency data for the round cartridge. Note the significant decrease in amplitude at 74 Hz for the round cartridge.

These tests confirmed that the out-of-round cartridge did cause the outer ring to distort, generating the 74 Hz axial motion and producing over 3x the disturbance at 74 Hz than bearings installed in the round cartridge.

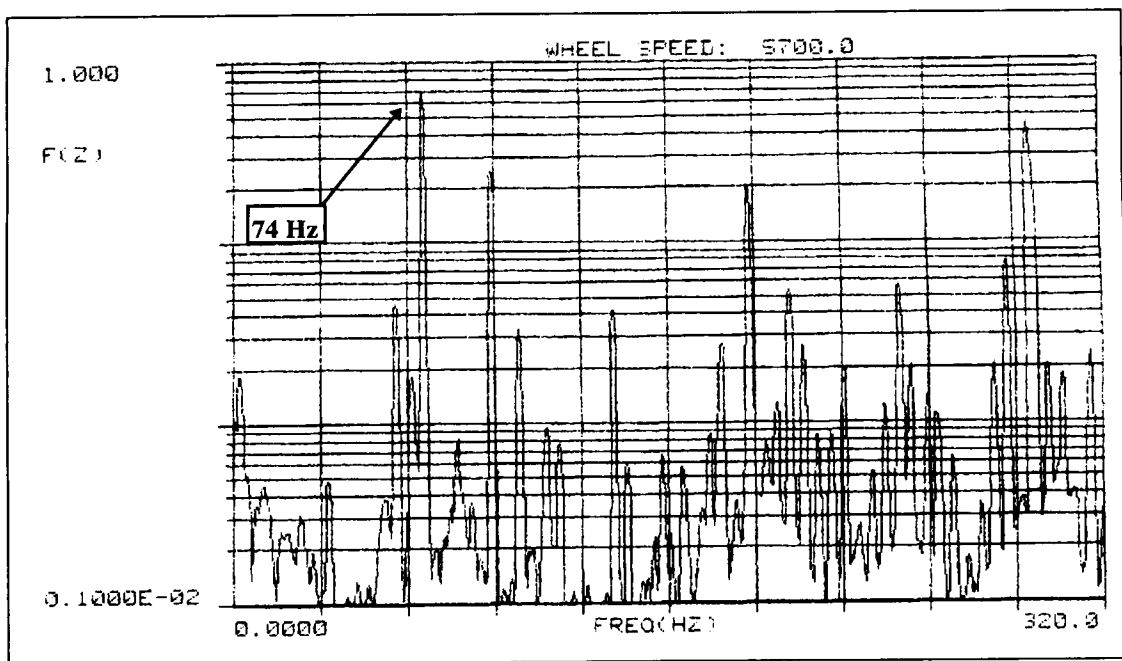


Figure 11. Out-of-round Cartridge

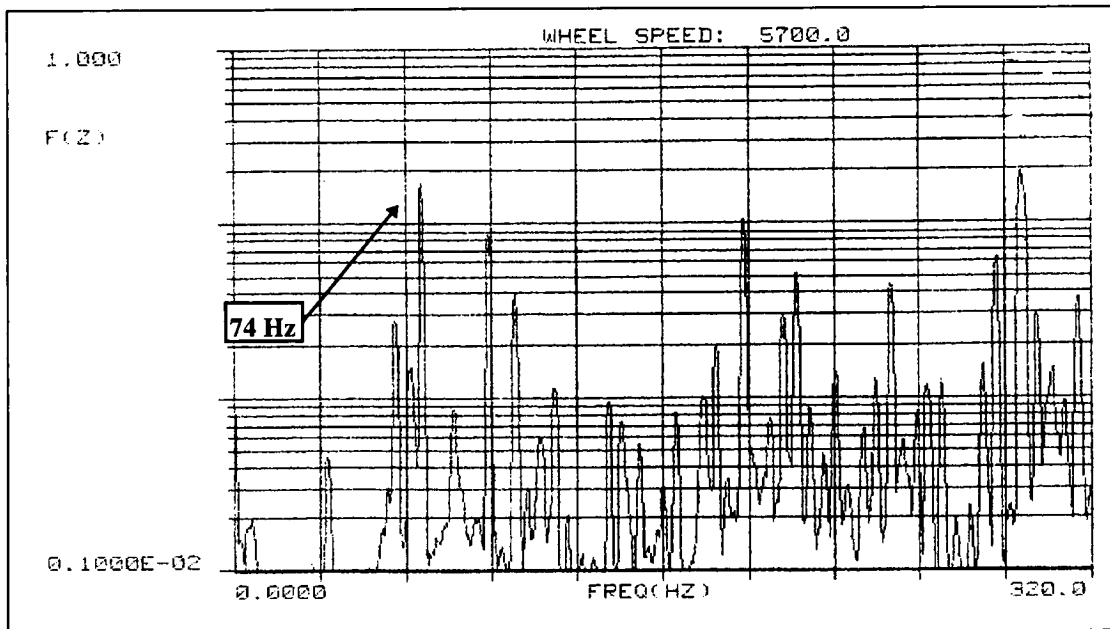


Figure 12. Round Cartridge

CONCLUSIONS

The quasi steady state model was successful in predicting the source of the 74 Hz axial disturbance. The effect of the cartridge out-of-round condition was the source of the undesirable motion. The bearing outer races that generated the 74 Hz disturbance were measured and found to have an interference with the out-of-round cartridge.

Placing the bearings in a round cartridge reduced the undesirable vibration. Placing the bearings back in the out-of-round cartridge reproduced the undesirable performance.

The Motion Model is a useful tool to predict bearing motion using theoretical or actual bearing geometric data.